Estimating the performance of wind turbines misaligned with respect to the wind direction using a simplified CFD based approach

Journal of Physics: Conference Series **2767** (2024) 022039 doi:10.1088/1742-6596/2767/2/022039

Estimating the performance of wind turbines misaligned with respect to the wind direction using a simplified CFD based approach

Sudipta Lal Basu, Breiffni Fitzgerald, Biswajit Basu
School of Engineering, Trinity College Dublin, College Green, Dublin 2, Ireland
E-mail: basus@tcd.ie, Breiffni.Fitzgerald@tcd.ie, basub@tcd.ie

Abstract. Wind direction in atmospheric boundary layer changes constantly. As such, the power extracted from the wind turbines in a wind farm is subjected to change. This change in wind direction impacts the wake pattern which in turn affects the power output of the downstream wind turbines. Empirical wind farm models are useful in such cases to assess the overall performance of the wind farms. However, the results provided by these models can be made more useful if fluid-structure interaction (FSI) effects are also considered. In the present work, we begin by looking at the potential flow model and the issues associated with it and used a modified model with constant vorticity to analyze the wind power available to the downstream wind turbines in a wind farm misaligned with respect to wind direction for irrotational flow. A simplified FSI based approach is used to carry out the simulations without the need of modelling the complicated wind turbine geometry.

1. Introduction

Wind direction in atmospheric boundary layer (ABL) is never constant. As such operation of wind turbines misaligned with respect to the wind direction is not uncommon. This phenomenon is commonly referred to as yaw. In reality yaw is a dynamic effect. However, the work carried out in this paper is not focussed on the dynamics and rather on the performance of back-to-back wind turbines in a wind farm in steady state under varying levels of misalignment. It is not unknown that excessive misalignment is detrimental to the operation of a wind turbine and hence, understanding the effects of misalignment is essential in designing the yaw controllers in order to ensure that the wind turbine rotor is aligned to the wind direction as much as possible within the prescribed yaw error. This in turn is essential to estimate the optimal power output. The continuous variation in wind direction makes wind turbine blades susceptible to higher fatigue loads which makes the study of this misalignment all the more important. Theoretical formulations for thrust and power coefficients of a misaligned wind turbine based on momentum theory or based on Glauert's Momentum theory are known. However, it is found that the axial momentum theory is more likely to estimate the power extraction correctly whereas Glauert's theory is more likely to estimate the thrust correctly [1].

With the advancement in computerised simulations, researchers have used Large Eddy Simulations to investigate the wind vector for yaw control [2] and even implemented artificial neural network (ANN) for yaw control [3]. These computer based methodologies are undoubtedly useful and provide a good insight into yaw operation during detailed engineering stage. However,

if one wants to study the implications of misalignment without going into the complicated computational fluid dynamics (CFD) based analysis like LES or ANN based deep learning studies which are usually known to be computationally expensive, particularly if the domain extends over hundreds of kilometers, simplified physical models (e.g. Jensen's model[4], Gaussian model[5]; to name a few) are helpful. However, compared to the detailed CFD models, which are more accurate and where fluid-structure interaction (FSI) effects are inherent, these simplified models do not consider these effects. Researchers have pointed out that special FSI methods can mitigate this issue without the requirement of modelling the structure in detail [6]. This is demonstrated in the past in the context of wind turbines where the turbines were treated as porous actuator discs [7]. This is where the relevance of the present work comes into picture where an effort to study back-to-back wind turbines misaligned with respect to the wind direction is carried out using a simplified physical model coupled with one of the special FSI methods.

Amongst the different simplified mathematical models used in the study of the wind farms, potential flow based models are widely used because of their simplicity. Researchers have worked on potential flow solutions for actuator discs [9]. Their model is based on Euler and continuity equations and included wake expansion and pressure variation across an annulus. Further, they proposed correction to axially induced velocity. They have stressed the fact that most existing models assume uniform axial flow. However, they illustrated in their work it is the absolute velocity $|\mathbf{V}|$ which is uniform rather than the axial velocity, which is non-uniform. Based on these potential flow solutions, others compared actuator disc and Joukowsky rotor flows and explored the need for a tip correction [10]. However, a laminar flow model with vorticity and wake interaction is something which has not been explored in detail in the case of wind turbines misaligned with wind direction and this is an area which is explored in this current work.

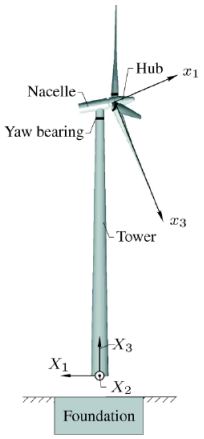

Figure 1: Co-ordinate system of three bladed wind turbine [8].

Thus, this study begins by understanding the relevance of the potential flow model in the context of these FSI methods before looking into the intricacies of the change in wind direction. In the current paper, an effort is made to implement one such special FSI approach (Decomposed Immersed Interface Method (DIIM) [11]) to study and compare the effects of variation in wind direction with the results available in literature. As can be understood, this work involves three major aspects:

- Understanding the limitations of a potential flow model with respect to DIIM and proposing a modified model
- Simulating the wind field under the influence of misaligned back-to-back wind turbines at time, $t = 0$ when all of them just start rotating from at rest condition as the cut-in wind speed is exceeded
- Computing the power available and comparing the same with the estimated power available as obtained from other models

2. Potential flow model

The reason for looking into the potential flow is its implementation in the context of wind farms in past works [10, 12, 13]. The velocity component parallel to a co-ordinate axis, X_j in terms of φ is defined by $\overline{V}_j = \varphi_{X_j} = \partial\varphi/\partial X_j; j \in \{1, 2, 3\}$ (refer Figure (1)). The potential flow model

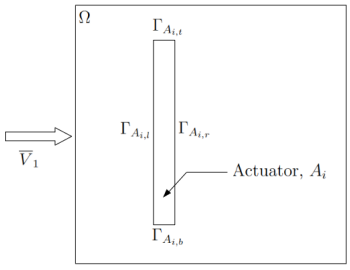

Figure 2: Schematic diagram of an actuator disc submerged in a fluid domain

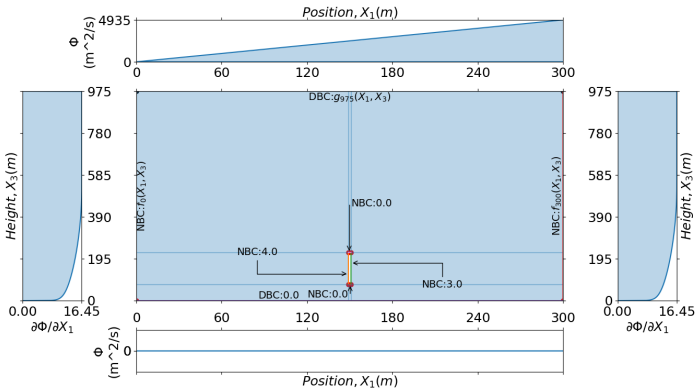

Figure 3: Geometrical model with potential, φ as dependent variable

takes the form

$$\frac{\partial^2 \varphi}{\partial X_i \partial X_i} = -b; b = 0; i \in \{1, 2, 3\} \tag{1}$$

2.1. Simulation model

A rectangular two-dimensional (2D) domain subjected to a shear flow in atmospheric boundary layer is considered. In the atmospheric boundary layer, the shear velocity function [14] is given by

$$\overline{V} = \frac{u_\tau}{\kappa'}\left(\ln\left(\frac{X_3}{z_0}\right) + 5.75\left(\frac{X_3}{h}\right) - 1.875\left(\frac{X_3}{h}\right)^2 - \frac{4}{3}\left(\frac{X_3}{h}\right)^3 + \frac{1}{4}\left(\frac{X_3}{h}\right)^4\right) \tag{2}$$

where, $\overline{V}$ = mean wind velocity parallel to earth's surface, κ' = von Karman's constant ≈ 0.4, ϕ = latitude of interest = 53.3498° for Dublin, Ω = rate of rotation of earth = $7.292 \times 10^{-5} rad/s$, C_D = drag coefficient taken approximately as 0.0014 for sea [15], u_τ = friction velocity = $M_{10}\sqrt{C_D} = M_{10}\sqrt{0.0014}$, f = coriolis parameter = $2\Omega \sin(\phi) = 1.17 \times 10^{-4} rad/s$ (for Dublin), h = gradient height = $u_\tau/6f$, M_{10} = wind speed at height of 10 m (considered $10m/s$), X_3 = height above MSL, z_0 = ground roughness length (Davenport-Wieringa roughness length = 0.0002 m for sea [15]).

2.2. Detailed analysis of the model

In 2D, say in $X_1 - X_3$ plane, the second order accurate central difference scheme when used to discretize eq.(1) takes the form

$$b_{i,j} - s\phi_{i,j} - p(\phi_{i+1,j} + \phi_{i-1,j}) - r(\phi_{i,j+1} + \phi_{i,j-1}) = 0. \tag{3}$$

where, $p = -\frac{1}{\triangle X_1^2}$, $r = -\frac{1}{\triangle X_3^2}$, $s = -2(p + r)$, $\triangle X_1$, $\triangle X_3$ are the node to node spacing in X_1 and X_3 direction respectively. Introducing the actuator discs into the domain makes it discontinuous and modifies the equation structure. Let A_i be an actuator submerged in a fluid domain, Ω containing multiple actuators (refer Figure (2)) where $i \in \{0, 1, 2, ...\}$ denotes the actuator number. Each actuator is bounded by $\Gamma_{A_{i,l}}$, $\Gamma_{A_{i,r}}$, $\Gamma_{A_{i,b}}$, $\Gamma_{A_{i,t}}$ on left, right, bottom and top respectively.

(i) **Geometrical model of the actuator disc and internal boundary conditions**

(a) One convenient option to model the actuator disc is to create an interior opening in the domain with height = diameter of the disc and thickness = average width of blade and assign Neumann Boundary Conditions (NBC) i.e. $\overline{V}_1 = \overline{V} = \varphi_{X_1}$ on $\Gamma_{A_{i,l}}$ and $\Gamma_{A_{i,r}}$ and $\overline{V}_3 = \varphi_{X_3}$ on $\Gamma_{A_{i,b}}$ and $\Gamma_{A_{i,t}}$. The values of φ_{X_1} can be assumed considering a reasonable value for axial induction factor, a. However, φ_{X_3} has to be based on some assumption (refer Figure (3)).

(b) Another option could be modelling the actuator as a solid disc of zero thickness with φ_{X_1} and φ_{X_3} in both directions at the grid points. In this case also, φ_{X_3} has to be based on some assumption. However, since the actuator thickness is zero, an abrupt change in the value of φ_{X_1} occurs as the velocity just in front of the actuator and just behind the actuator are different as per the actuator disc theory. Numerically, this would require some sort of smoothening function to mitigate.

Nonetheless both these options give rise to an internal closed boundary with all boundaries having NBC which is numerically known to result in a non-convergent solution of the sparse linear system given by eq.(3). This requires modelling the discontinuity ensuring that φ is known on at least one interior boundary for each such actuator. However, the relation between the values of φ for each of these actuators is unknown.

(ii) **External boundary conditions:** The actuator disc theory assumes no inflow or outflow from the top and the bottom boundaries. Hence, the following boundary conditions for the external boundaries might seem obvious.

(a) Bottom boundary: $\overline{V}_1\big|_{X_3=0} = \varphi_{X_1} = 0; \overline{V}_3\big|_{X_3=0} = \varphi_{X_3} = 0.$

$$\varphi = \int \varphi_{X_1} dX_1 = \int 0 dX_1 = f(X_3); \varphi \quad = \int \varphi_{X_3} dX_3 = \int 0 dX_3 = f(X_1)$$

which is possible if and only if $\varphi = f(X_3) = f(X_1) = k$, where k = constant i.e. Dirichlet Boundary Conditions (DBC) can be specified for φ

(b) Top boundary: The top boundary can be assigned boundary conditions in two ways:

1. Assigning NBC with $\varphi_{X_3}\big|_{X_3=H} = 0$; where H = overall height of the fluid domain considered.
2. Additionally, if it is assumed that at such a far off height, $\overline{V}_1$ ideally remains the same throughout i.e. $\varphi_{X_1}\big|_{X_3=H} = \overline{V}_{1,H}(X_3)$ (where $\overline{V}_{1,H}$ is the mean velocity at height H), then just like the bottom boundary DBC can be defined in this case as well.

$$\varphi = \int \varphi_{X_1} dX_1 = \int \overline{V}_{1,H} dX_1 = \overline{V}_{1,H} X_1 + f(X_3); \varphi = \int \varphi_{X_3} dX_3 = f(X_1)$$

Equating the above two equations give $\varphi = \overline{V}_{1,H} X_1$.

If for top boundary, only NBC is assumed, there is no concern. But, if DBC is considered for the top boundary and which is the more accurate condition, the issue is that the relation between $\varphi = k$ and $\varphi = \overline{V}_{1,H} X_1$ is not known.

(c) Left and right boundaries: For these two boundaries, since the mean velocity profile is known, the boundary conditions can be NBC with $\varphi_{X_1}\big|_{X_1=0} = \varphi_{X_1}\big|_{X_1=B} = \overline{V}_1(X_3)$, where B = overall width of the domain.

Now, even if the boundary conditions are assigned as stated above, few other problems still need to be addressed.

(a) Assigning DBC = k at the bottom boundary does not ensure that numerical simulation would yield $\overline{V}_3\big|_{X_3=0} = 0$. One way around this is to impose NBC = 0 additionally. In other words, Cauchy Boundary Condition (CBC) needs to be provided at the bottom boundary. Same holds true for the top boundary.

(b) Also, the effect of the velocity components tangential to the domain boundary has no effect on the solution of the velocity field.

(iii) **Compatibility at corner nodes:** With only one parameter φ governing the values of both $\overline{V}_1$ and $\overline{V}_3$, another issue is the complexity in satisfying the compatibility at the corner nodes of the domain. The values of φ assumed at the boundary nodes should be such that the value for $\overline{V}_1$ w.r.t. both boundaries forming the corner should also satisfy the requirement of $\overline{V}_3$. It is difficult to ensure that all these criteria are satisfied at the same time and numerically these would introduce great many constraints in the problem definition.

3. Model reformulation

The idea presented in this section is influenced by [16] and validation of the code incorporating DIIM developed by the authors was presented in [7]. Differentiating the equation of continuity w.r.t. X_1 and the equation for vorticity w.r.t. X_3, the following equations are obtained.

$$\frac{\partial^2 \overline{V}_1}{\partial X_1^2} + \frac{\partial^2 \overline{V}_3}{\partial X_1 \partial X_3} = 0; \quad \frac{\partial^2 \overline{V}_3}{\partial X_3 \partial X_1} - \frac{\partial^2 \overline{V}_1}{\partial X_3^2} = \boldsymbol{\omega}_{X_3} \tag{4}$$

Subtracting these two equations, a PDE for $\overline{V}_1$ is obtained.

$$\frac{\partial^2 \overline{V}_1}{\partial X_1^2} + \frac{\partial^2 \overline{V}_1}{\partial X_3^2} = -\boldsymbol{\omega}_{X_3} \tag{5}$$

Similarly, differentiating the equation of continuity w.r.t. X_3 and the equation for vorticity w.r.t. X_1, the following equations are obtained.

$$\frac{\partial^2 \overline{V}_1}{\partial X_3 \partial X_1} + \frac{\partial^2 \overline{V}_3}{\partial X_3^2} = 0; \quad \frac{\partial^2 \overline{V}_3}{\partial X_1^2} - \frac{\partial^2 \overline{V}_1}{\partial X_1 \partial X_3} = \boldsymbol{\omega}_{X_1} \tag{6}$$

Again, adding these two equations, a PDE for $\overline{V}_3$ is obtained.

$$\frac{\partial^2 \overline{V}_3}{\partial X_1^2} + \frac{\partial^2 \overline{V}_3}{\partial X_3^2} = \boldsymbol{\omega}_{X_1} \tag{7}$$

The advantages of this new formulation are

(i) **Geometrical model of actuator disc:** Since two elliptic PDEs are now available with $\overline{V}_1$ and $\overline{V}_3$ as dependent variables, there is no need to consider NBC at the boundaries because the velocity functions are known at the boundaries straightaway.

(ii) **Boundary conditions:** Unlike the case with the potential flow model, where some arbitrary value for potential is required to be imposed in order to start the simulations and where CBC is needed to satisfy the criteria for both $\overline{V}_1$ and $\overline{V}_3$ at the boundaries making the system more rigid, the current formulation is far more flexible.Also, there is no need to think about the gradient of the dependent variable parallel to the boundaries as it has no physical implication as such.

(iii) **Compatibility at corner nodes:** Since two separate PDEs are getting solved and DBC are known at the boundaries straightaway, there is no need to check for compatibility at the corner nodes as such.

(iv) **A more general model:** The interaction between the air (fluid) and the aerofoil (structure) is responsible for the vortex formation. However, modelling the aerofoil itself or the blade is computationally expensive. The model presented in this work is an attempt

to inculcate this fluid-structure interaction by using an approach (Decomposed Immersed Interface Method (DIIM) [11]) which is computationally less intensive compared to the standard blade resolved CFD models and without the need for modelling the actual aerofoil but at the same time including its effects by applying appropriate boundary conditions at the interface of the actuator disc and the fluid domain. Hence, this formulation can be applied to both irrotational and rotational flow problems.

4. Simulations and Results

For misaligned wind turbines, we look in $X_1 - X_2$ plane at the hub level ($d_0 = 150m$) such that $\overline{V} = 14.0026m/s$ (from eq.(2)) with zero vorticity. In Figure (4), we have $\overline{V}_1 = \overline{V}\cos\theta$ and $\overline{V}_2 = \overline{V}\sin\theta$. Three back-to-back actuators of $150m$ diameter each are considered installed approximately seven rotor diameters ($1000m$) from one another. A length of $1000m$ is considered upstream of the first actuator and a length of $1000m$ is considered downstream of the last actuator i.e. $X_1 = 4000m$. A length of five times the diameter of actuator disc is considered on either side of the actuator and thus, the width of the domain is $X_3 = 1700m$. The actuators are modelled as a rectangle using DIIM wherein the actuator is considered as an energy extracting porous disc with known jumps or change in velocity along the interface separating the actuator from the overall fluid domain. With an axial induction factor of $a = 1/3$, the jump in front of the first actuator, A_0 comes out to be $[\overline{V}_1] = \overline{V}\cos\theta/3 = 14.0026\cos\theta/3 = 4.6675\cos\theta m/s$. The jump at all the other interfaces are considered to be zero. For the downstream actuators, A_1 and A_2, the jump is computed using Jensen's wind farm model where, $k = r_0/(r_0 + \alpha x_0) = 0.4286, \alpha = 0.1, r_0 = d_0/2$. Thus,
For A_1: $v_1/\overline{V}_1 = [1 - 2/3.k^2] = 0.8775; [\overline{V}_1]_1 = (1 - 0.8775)\overline{V}_1 = 0.1225\overline{V}_1$
For A_2: $v_2/\overline{V}_1 = 1 - [1 - 1/3.v_1/\overline{V}_1]k^2 = 0.8700; [\overline{V}_1]_2 = (1 - 0.8700)\overline{V}_1 = 0.13\overline{V}_1$
where, v_i =velocity just upstream of actuator A_i; $i \in \{0, 1, 2\}$ numbered from left to right in Figure (4). At the right boundary, the velocity within the expanded wake region, v_3 is considered such that $v_3/\overline{V}_1 = 1 - [1 - 1/3.v_2/\overline{V}_1]k^2 = 0.8696$. For equation of continuity to be satisfied, the velocity in the zone outside the expanded wake is computed using

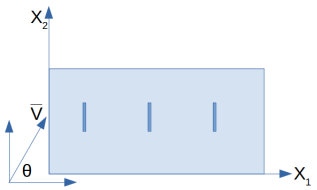

Figure 4: Arrangement of actuators

$$A_{exp}v_3 + A_{out}v' = A_{left}\overline{V}_{1,left} \tag{8}$$

where, $A_{exp}, A_{out}, A_{left}$ are area of cross-section of the expanded wake at the right boundary, outside the expanded wake at the right boundary and at the left boundary respectively, v' is the velocity outside the expanded wake on the right boundary. As the actuator is a thin disc, no change in the velocity component, $\overline{V}_2$ occurs and thus, $[\overline{V}_2] = 0$. The simulations are carried out for misalignments varying from 0^o to 20^0 at an interval of 5^o. Yaw controllers usually restrict the yaw of a wind turbine within $20^o - 30^o$ [17, 18, 19]. For this reason, the misalignments for the simulations carried out in this work are restricted within 20^o. The boundary conditions and the jumps for the simulations carried out are presented in Table 1.

Comparison with Jensen's model

The results of the simulation for $\overline{V}_1$ are presented in Figure (5) and the wind power available immediate upstream of the downstream actuators are presented in Table 2. For the purpose of comparison, the average value $\overline{V}_1$ is computed as per Jensen's model for the downstream actuators and is presented in Table 2. It can be observed that these theoretical values of $\overline{V}_1$ obtained as per Jensen's model match approximately with the average value of $\overline{V}_1$ obtained from the numerical simulations (with a variation ranging from $8\% - 9\%$). These results justify that the model presented is an acceptable approach.

Table 1: Jumps and boundary conditions at different misalignments

Misalignment, θ^o	$\overline{V}_1$ (m/s)	$[\overline{V}_1]_0$ (m/s)	$[\overline{V}_1]_1$ (m/s)	$[\overline{V}_1]_2$ (m/s)	v_3 (m/s)	v' (m/s)
0	14.0026	4.6675	1.7153	1.8203	11.6793	14.0027
5	13.9493	4.6498	1.7088	1.8134	11.6348	13.9741
10	13.7898	4.5966	1.6893	1.7927	11.5019	13.8143
15	13.5254	4.5085	1.6119	1.7106	11.2813	13.5495
20	13.1581	4.3860	1.6569	1.7583	10.9749	13.1815

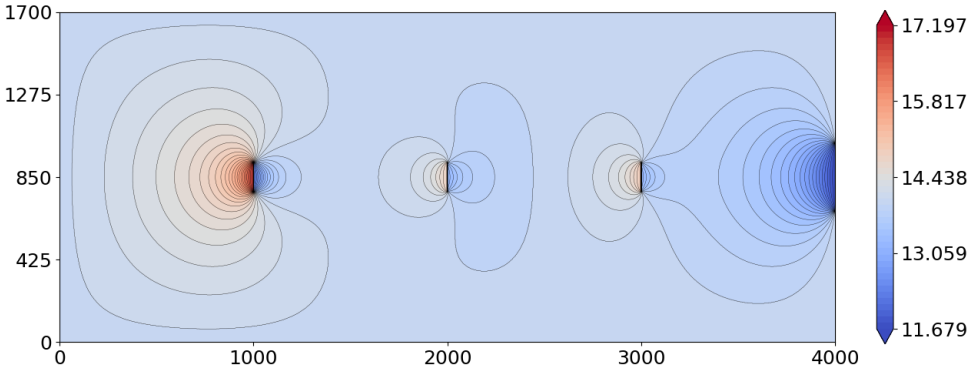

(a) $\theta = 0^o$

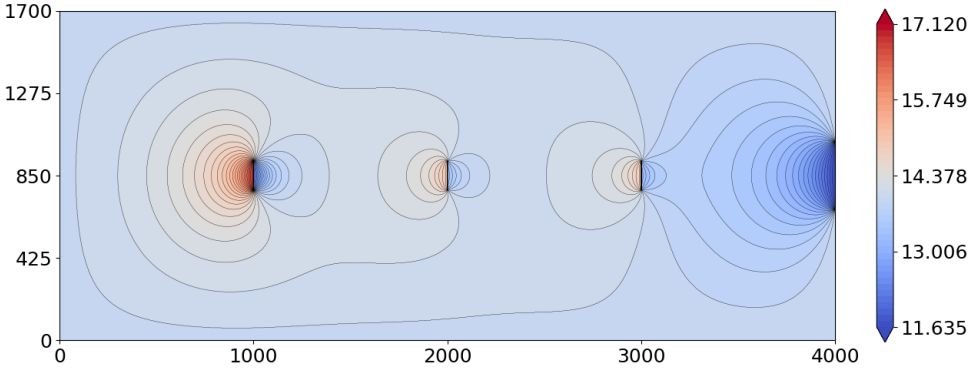

(b) $\theta = 5^o$

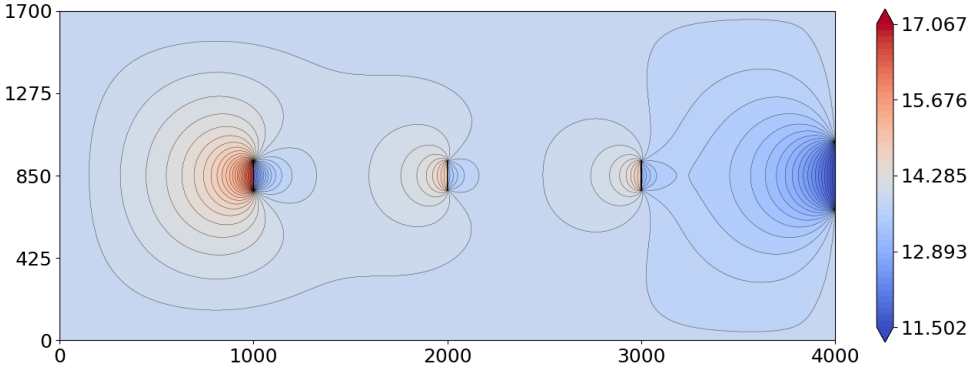

(c) $\theta = 10^o$

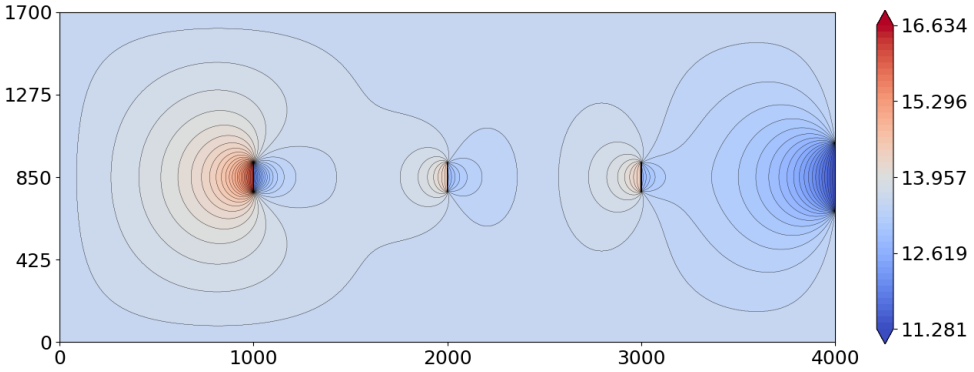

(d) $\theta = 15^o$

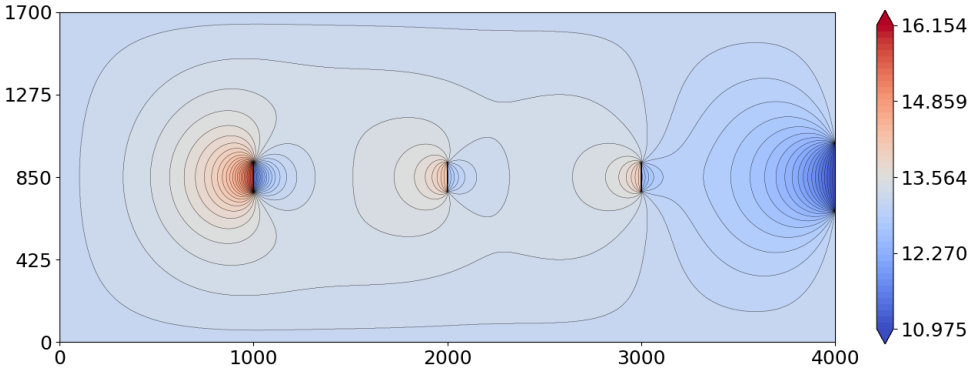

(e) $\theta = 20^o$

Figure 5: Contour of $\overline{V}_1$ at different misalignments

Table 2: Available wind power

θ^o	$P_F(\times 10^6)$ $(\propto \overline{V}^3_{1,left})$	$\overline{V}_{1,1}$ (Jen.)	$\overline{V}_{1,1}$ (Num.)	$P_1(\times 10^6)$ $(\propto \overline{V}^3_1)$	P_{P1}	$\overline{V}_{1,2}$ (Jen.)	$\overline{V}_{1,2}$ (Num.)	$P_2(\times 10^6)$ $(\propto \overline{V}^3_1)$	P_{P2}
0	48.41	12.29	13.21	40.49	0.84	12.18	13.24	40.70	0.84
5	47.86	12.24	13.41	42.28	0.88	12.14	13.20	40.35	0.84
10	46.23	12.10	13.28	41.15	0.89	12.00	13.09	39.35	0.85
15	43.62	11.87	12.83	37.03	0.85	11.77	12.80	36.79	0.84
20	40.17	11.55	12.70	35.92	0.89	11.45	12.48	34.09	0.85

P_F: Free stream power (in Watts), P_i: Wind power (in Watts) available upstream of actuator, A_i, P_{Pi}: fraction of useful wind power w.r.t. P_F available upstream of A_i, $\overline{V}_{1,i}$: $\overline{V}_1$ at A_i, Jen.: as per Jensen's model, Num.: as per numerical analysis

It can be observed that the wind power available for A_1 shows a decrease which is about $84\% - 89\%$ and for actuator A_2, a decrease which is about $83\% - 85\%$ with respect to the free stream wind power for all the five cases simulated. Possible reason for this could be that there are no more actuators further downstream of A_2 and the wind velocity starts getting back to the free-stream velocity. Further, the introduction of FSI into the model could be yet another reason for this behaviour.

5. Conclusion

In the present work, a simplified CFD based approach to estimate the performance of wind turbines misaligned with respect to the wind direction is presented. A detailed analysis of the potential flow model has been carried out and the different problems associated with the same are highlighted. A new model is proposed which not only overcomes most of the issues faced by the potential flow model but also is capable of modelling flows with vorticity as well. Simulations are carried out and results compared with Jensen's wind farm model which illustrates that the proposed approach gives acceptable results. Additionally, the proposed approach is capable of inculcating the FSI effects into the analysis. As expected, it is observed that with the increasing misalignment, the wind power available for the downstream wind turbines to be extracted goes on reducing which demonstrates that the proposed model is acceptable. The simulations presented in this work assume that all the wind turbines have the same degree of misalignment. However, it does not restrict the applicability of the proposed model to scenarios where each wind turbine is misaligned at different degree. If the velocity component $\overline{V}_2$ is simulated and the resultant velocity plotted, the wake deflection can also be observed. In future, the work can be further extended to include time in the model so that yaw, as a dynamic phenomenon, can also be accommodated by the model.

Acknowledgments

This work is supported by Science Foundation Ireland (SFI) grant no. 20/FFP-P/8702.

References

[1] T. Burton et al. *Wind energy handbook*. John Wiley and Sons, 2011. ISBN: 978-0-470-69975-1.

[2] G. Cortina, V. Sharma, and M. Calaf. "Investigation of the incoming wind vector for improved wind turbine yaw-adjustment under different atmospheric and wind farm conditions". In: *Renewable Energy* 101 (2017), pp. 376–386. DOI: 10.1016/j.renene.2016.08.011.

[3] A. Saenz-Aguirre et al. "Artificial Neural Network Based Reinforcement Learning for Wind Turbine Yaw Control". In: *Energies* 12.3 (2019). DOI: 10.3390/en12030436.

[4] N.O. Jensen. "A note on wind generator interaction". In: *Risø-M No. 2411*. Risø National Laboratory, 1983, pp. 1–18.

[5] M. Bastankhah and F. Porté-Agel. "A new analytical model for wind-turbine wakes". In: *Renew. Energy* 70 (2014), pp. 116–123. DOI: 10.1016/j.renene.2014.01.002.

[6] R. Mittal and G. Iaccarino. "Immersed Boundary Methods". In: *Annual Rev. of Fluid Mech.* 37.1 (2005), pp. 239–261. DOI: 10.1146/annurev.fluid.37.061903.175743.

[7] S.L. Basu et al. "Flow in a large wind field with multiple actuators in the presence of constant vorticity". In: *Phys. of Fluids* 34.10 (Oct. 2022). DOI: 10.1063/5.0104902.

[8] S.R.K. Nielsen. "Aerodynamics of Wind Turbines". University Lecture. 2017.

[9] G. A. M. van Kuik and L. E. M. Lignarolo. "Potential flow solutions for energy extracting actuator disc flows". In: *Wind Energy* 19.8 (2016), pp. 1391–1406.

[10] G. A. M. van Kuik et al. "Comparison of actuator disc and Joukowsky rotor flows, to explore the need for a tip correction". In: *J. of Phys.: Conf. Series* 625 (2015), p. 012013.

[11] P.A. Berthelsen. "A decomposed immersed interface method for variable coefficient elliptic equations with non-smooth and discontinuous solutions". In: *J. of Comput. Phys.* 197.1 (2004), pp. 364–386. DOI: 10.1016/j.jcp.2003.12.003.

[12] G. Xu and L. Sankar. "Computational study of horizontal axis wind turbines". In: *37th Aerospace Sci. Meeting and Exhibit.* 2000, pp. 35–39.

[13] G. Xu and L. Sankar. "Effects of transition, turbulence and yaw on the performance of horizontal axis wind turbines". In: *2000 ASME Wind Energy Symposium*. 2000, pp. 259–265.

[14] P.J. Richards and S.E. Norris. "Appropriate boundary conditions for computational wind engineering: Still an issue after 25 years". In: *J. of Wind Eng. and Industrial Aerodyn.* 190 (2019), pp. 245–255. DOI: 10.1016/j.jweia.2019.05.012.

[15] R. Stull. *Practical Meteorology: An Algebra-based Survey of Atmospheric Science*. AVP International, University of British Columbia, 2016, pp. 687–721. ISBN: 0888651767.

[16] B. Basu. "Irrotational two-dimensional free-surface steady water flows over a flat bed with underlying currents". In: *Nonlinear Anal.: Theory, Methods & Applications* 147 (2016), pp. 110–124. DOI: 10.1016/j.na.2016.08.016.

[17] P.M.O. Gebraad et al. "Wind plant power optimization through yaw control using a parametric model for wake effects—a CFD simulation study". In: *Wind Energy* 19.1 (2016), pp. 95–114. DOI: 10.1002/we.1822.

[18] Z. Xin et al. "Numerical Study on the Yaw Control for Two Wind Turbines under Different Spacings". In: *Appl. Sci.* 12.14 (2022). DOI: 10.3390/app12147098.

[19] M. Bastankhah and F. Porté-Agel. "Wind farm power optimization via yaw angle control: A wind tunnel study". In: *J. of Renew. and Sustain. Energy* 11.2 (Mar. 2019), p. 023301. DOI: 10.1063/1.5077038.